RSC Advances

PAPER

View Article Online
View Journal | View Issue

Check for updates

Cite this: *RSC Adv.*, 2017, **7**, 54468

One pot synthesis of NiMo–Al_2O_3 catalysts by solvent-free solid-state method for hydrodesulfurization†

Xiaodong Yi,* Dongyun Guo, Pengyun Li, Xinyi Lian, Yingrui Xu, Yunyun Dong, Weikun Lai and Weiping Fang

A simple and solvent-free solid-state method was used to prepare NiMo–Al_2O_3 hydrodesulfurization (HDS) catalysts using $Ni(NO_3)_2 \cdot 6H_2O$, $(NH_4)_6Mo_7O_{24} \cdot 4H_2O$, and $AlCl_3 \cdot 6H_2O$ as the solid raw materials and polyethylene glycol (PEG) as an additive. The effects of PEG addition on the precursor thermal decomposition, catalyst properties and dibenzothiophene (DBT) HDS activity were investigated. The as-prepared catalysts were characterized by nitrogen adsorption–desorption measurements, powder X-ray diffraction (XRD), thermogravimetric analysis/differential scanning calorimetry (TGA/DSC), H_2 temperature-programmed reduction (H_2-TPR), X-ray photoelectron spectroscopy (XPS), scanning electron microscopy (SEM) and high resolution transmission electron microscopy (HRTEM). The results showed that an increase in PEG addition dramatically increases specific surface area and pore volume of the catalyst, and improves Mo sulfidability and active MoS_2 dispersion by blocking the aggregation of metals, and consequently increases the number of HDS active sites. However, excess PEG leads to the decrease in specific surface area and pore volume attributed to the metal sintering caused by the strong heat release during thermal decomposition. As a result, dibenzothiophene HDS activity enhanced with increasing PEG addition and peaked at NiMoAl-15 (15% weight ratio of PEG to alumina), which exhibited a significantly higher activity as compared to the NiMo/Al_2O_3 catalyst prepared by wetness co-impregnation.

Received 29th October 2017
Accepted 24th November 2017

DOI: 10.1039/c7ra11892a

rsc.li/rsc-advances

Open Access Article. Published on 27 November 2017. Downloaded on 2/15/2026 4:36:53 AM.
This article is licensed under a Creative Commons Attribution 3.0 Unported Licence.

1. Introduction

Due to increasingly stringent environmental regulations for the sulfur content in fuel oils,[1] catalytic hydrodesulfurization (HDS) is widely used to remove sulfides in petroleum refining. In typical commercial HDS catalysts, active components MoS_2(WS_2) and Co(Ni) promoters are supported on γ-alumina. The HDS activity of the multicomponent catalysts depends on the synthetic procedure and their compositions. In recent years, different supporters such as SiO_2, ZrO_2, TiO_2 and mixed oxides have been widely studied for improving HDS performance.[2–5] Another source of activity enhancement can be an alternative active phase based on transition metals (*e.g.*, Ru, Fe, Rh, Pt) or carbides, phosphides.[6–8] In addition, the addition of different organic compounds such as ethylene diamine tetraacetic acid (EDTA), citric acid, thioglycolic acid or polyethylene glycol also has crucial influence.[9–12]

Many approaches have been employed to improve metal dispersion of the catalysts for high HDS activity. The commonly used HDS catalyst preparation methods include simultaneous or sequential impregnation, hydrothermal deposition and sol–gel synthesis.[13–15] For these methods, a complicated and time-consuming process is always required and active metal components on the support surface tend to agglomerate into large crystallites. Therefore, a novel and efficient solid-state reaction for preparing metal complexes, metal oxides or sulfides with uniform sizes and shapes has been developed. Zhang *et al.* reported a low-temperature solid-state reaction for the synthesis of ammonium aluminum carbonate hydroxide (AACH), which used poly-glycol (PEG), NH_4HCO_3 and $Al(NO_3)_3 \cdot 9H_2O$ as precursors.[16] The alumina obtained by the calcination of AACH showed unique bimodal porous structure and high content of surface acid. Without any solvents, Ren *et al.* synthesized zeolites with MFI structure by mechanically mixing of solid raw materials.[17] Because of the simple, rapid, solvent-free and energy-saving process, this method has attracted extensive research interest.

Recently, solid-state reaction has been applied to the synthesis of supported catalysts with a high dispersion of active metal, in which solid state reactions occur between hydrated transition metal salts and organics. With this method, Cu/ZnO/

National Engineering Laboratory for Green Chemical Productions of Alcohols, Ethers and Esters, College of Chemistry and Chemical Engineering, Xiamen University, Xiamen 361005, P. R. China. E-mail: xdyi@xmu.edu.cn

† Electronic supplementary information (ESI) available. See DOI: 10.1039/c7ra11892a

This journal is © The Royal Society of Chemistry 2017

Open Access Article. Published on 27 November 2017. Downloaded on 2/15/2026 4:36:53 AM. This article is licensed under a Creative Commons Attribution 3.0 Unported Licence.

ZrO_2 catalysts were prepared for CO_2 hydrogenation; the copper dispersion and catalytic activity of the catalysts are strongly influenced by calcination temperature.[18] Our group systematically studied the properties of NiMo–Al_2O_3 catalysts prepared by a similar process using starch and urea as additive.[19,20] The results showed that an appropriate concentration of starch improves the HDS activity, but an excess of starch addition decreases the activity because of agglomeration of Mo particles. Compared with conventional impregnation method, introducing active metal during the synthesis process of mesoporous alumina possesses especial advantages, including high dispersion of metallic composition and preferable anti-sintering.

As mentioned, such solid-state method has seldom been used to load active metal components and synthesis carrier in a one-step process, particularly in using this method to prepared supported HDS catalyst. Herein, we report the solvent-free solid-state synthesis of NiMo–Al_2O_3 catalysts using PEG as additive. The solid-state reaction is not only used for producing alumina but also used for dispersing Ni–Mo active species onto the support simultaneously. A detailed study on the influence of PEG addition on the catalytic behavior of NiMo–Al_2O_3 catalyst for dibenzothiophene (DBT) hydrodesulfurization has been performed.

2. Experimental section

2.1. Synthesis samples

$Ni(NO_3)_2 \cdot 6H_2O$, $(NH_4)_6Mo_7O_{24} \cdot 4H_2O$, $AlCl_3 \cdot 6H_2O$ and alkapolpeg-6000 (PEG-6000, molecular weight: 6000) were purchased from Sinopharm Chemical Reagent (China). Commercial alumina (γ-Al_2O_3, SSA 260 m^2 g^{-1}) was obtained from Fushun Research Institute of Petroleum and Petrochemical, SINOPEC, Fushun, China. All of the above chemicals were used as purchased without any further purification.

A series of NiMo–Al_2O_3 catalysts with different PEG addition were prepared by solid-state synthesis. In a typical preparation, the solid raw materials $Ni(NO_3)_2 \cdot 6H_2O$, $(NH_4)_6Mo_7O_{24} \cdot 4H_2O$, $AlCl_3 \cdot 6H_2O$ and PEG-6000 (molecular weight: 6000) were mixed and grinded at ambient temperature for 10 min, then calcined at 500 °C at a heating rate of 10 °C min^{-1} for 4 h in muffle furnace. The samples were denoted as NiMoAl-x ($x = 0$, 2, 6, 10, 15 and 20), where x represents the weight ratio of PEG to alumina. In the final catalyst, the content of MoO_3 and NiO are 12 wt% and 4 wt%, respectively.

For comparison, commercial alumina (γ-Al_2O_3, SSA 260 m^2 g^{-1}) supported NiMo catalyst have been prepared by co-impregnation of aqueous solutions of ammonium heptamolybdate and nickel nitrate. The catalyst precursor was dried at 110 °C for 12 h, followed by calcining at 500 °C for 5 h, and the final catalysts were denoted as NiMo/Al_2O_3. The content of MoO_3 and NiO in the final catalyst was the same as the catalyst prepared by solid-state synthesis method.

2.2. Characterization

Thermogravimetric analysis/differential scanning calorimetry (TGA/DSC) of the precursor before calcination was conducted in flowing air atmosphere up to 800 °C at a heating rate of 10 °C min^{-1} with TGA/DSC (SDT Q600) thermal analyzer.

Nitrogen adsorption–desorption measurements of the catalysts were performed on a Micromeritics Tristar 3000 adsorption automatic instrument at liquid nitrogen temperature. The samples were outgassed at 300 °C for 3 h in vacuum. Surface areas were calculated by the Brunauer–Emmett–Teller (BET) method, and the pore size distribution and total pore volume were determined by the Barrett–Joyner–Halenda (BJH) method.

Powder X-ray diffraction (XRD) characterization was carried out on an X'Pert Pro automatic powder diffractometer operated at 40 kV and 30 mA using CuKα (λ = 0.15406 nm) monochromatized radiation in all cases.

Temperature-programmed reduction (TPR) experiments were performed with a GC-TPR apparatus. The samples of as-made NiMoAl-x (50 mg) were pretreated in an Ar stream at 300 °C for 1 h and then cooled to room temperature. Next, the catalyst was heated to 900 °C at a rate of 10 °C min^{-1} under a 30 ml min^{-1} flow of an 5% H_2/Ar mixture. H_2 consumption was determined by a thermal conductivity detector (TCD).

XPS spectra were obtained in MultiLab 2000 spectrometer using Mg Kα radiation under vacuum (<10^{-9} mbar). The oxidic catalysts were pressed into thin sheets, sulfurized in a 15% H_2S/H_2 stream at 400 °C for 2 h, and then cooled to room temperature. Before measurement, the sulfided catalysts were kept under inert atmosphere without contact air.

Scanning electron microscopy (SEM) images were obtained on a field emission scanning electron microscopy LEO-1530 device, which was manufactured by Leo Company in Germany. Emission voltage was 15 eV, and accelerating voltage was 20 kV.

High-resolution transmission electron microscopy (HRTEM) images of the samples were obtained using a Philips Analytical FEI Tecnai 30 electron microscope operating at 300 kV. Freshly sulfided catalyst was ultra-sonically dispersed in ethanol. The suspension was then collected on a car bon-coated copper grid.

2.3. Catalytic tests

Dibenzothiophene (DBT) HDS reaction was measured in a high-pressure fixed-bed continuous-flow stainless steel reactor with internal diameter 6.0 mm. Before the reaction, the catalyst was sulfurized *in situ* at 400 °C for 2 h in a stream of 15 vol% H_2S/H_2 under atmospheric pressure. The reaction protocol is as follows: 300 °C with a total pressure of 2.0 MPa, a liquid hourly space velocity (LHSV) of 12 h^{-1}, and a H_2/hydrocarbon volumetric ratio of 600, using 2.0 wt% DBT in decalin as a model compound. The liquid product was collected every hour after a steady state had been reached and analyzed by a gas chromatograph equipped with a FID detector and a HP-5 capillary column. The GC spectra and product distribution of DBT HDS were shown in S-Fig. 1.†

3. Result and discussion

3.1. Thermal analysis

Thermal oxidative decomposition of the various precursors, which determines the structure and property of the resultant

Open Access Article. Published on 27 November 2017. Downloaded on 2/15/2026 4:36:53 AM. This article is licensed under a Creative Commons Attribution 3.0 Unported Licence.

catalyst, is significantly affected by the PEG addition. The thermal analysis results for the NiMoAl-*x* precursors with different PEG contents are reported in Fig. 1. As seen from TG curves in Fig. 1A, the weight loss for NiMoAl-*x* at about 100 °C corresponds to the removal of moisture. The major weight loss for NiMoAl-*x* between 150 °C and 350 °C is attributed to a series of overlapping oxidative decomposition reactions, including the process of dehydration–decomposition and dehydroxylation of PEG and aluminum chloride and the subsequent total transformation of nickel nitrate and ammonium heptamolybdate.[21,22] The presence of PEG exhibits a new weight loss at 300 °C, while it becomes greater with the increase of PEG content. The total weight losses coincided with the expected values, indicating that both the PEG and the precursors are completely decomposed.

As shown in Fig. 1B, the DSC curves indicate several endothermic processes at temperature lower than 250 °C and an exothermic reaction at higher temperature. A weak endothermic band occurs at 60 °C for PEG-containing samples corresponds to the melting of the extended chains, the other endothermic peak locates in 100–250 °C is caused by the partial thermal decomposition of the precursors. Whereas, a strong exothermic peak at about 300 °C is assigned to the combustion decomposition of PEG, in this process, most of aluminium chloride is decomposed into oxide. With the increasing PEG addition, the exothermic peak area and peak height at 300 °C increase proportionally. Otherwise, most of the chloride ion is removed as gaseous HCl or NH_4Cl during the calcining process, but there is still a trace residual on the oxide catalysts. Interestingly, we have not detected the presence of Cl on the sulfide catalysts, which might generate HCl during the sulfidation process (Table S1†).

3.2. Textural properties and crystalline phase

Nitrogen adsorption–desorption isotherms of the NiMoAl-*x* catalysts are shown in Fig. 2A. All the samples exhibit type IV isotherms with H1 hysteresis loops, which indicate the feature of mesoporous structure. The area of the hysteresis loops and quantity of N_2 adsorbed for the NiMoAl-*x* samples increase significantly with increasing PEG addition, which indicates that the porous system develops as PEG content increases. Texture parameters calculated by BET and BJH methods (Table 1) show that the BET surface area and pore volume increase obviously with increasing PEG addition. However, when the PEG addition is sufficiently high, comparing to the NiMoAl-15 sample, the BET surface area and pore volume of NiMoAl-20 decrease. On the one hand, swelling is not completely free, but is constrained by steric effects; on the other hand, the considerable heat released *via* roasting excessive amount of PEG results to the agglomeration of nickel–molybdenum particles. Pore size distribution in Fig. 2B shows that the most probable pore size improves with increasing PEG content, yielding a wide pore size distribution. Meanwhile, a series of Al_2O_3-*x* (where *x* represents the weight ratio of PEG to alumina, and $x = 0, 10, 15, 20$) were synthesized *via* solvent-free solid-state route with different PEG addition (Table S2 and S-Fig. 2†). All these results indicate that PEG plays a key role in directing framework of the as-prepared catalyst.

X-ray diffraction patterns of the oxide (A) and sulfide (B) NiMoAl-*x* catalysts are shown in S-Fig. 3.† For the oxide catalysts, a weak peak corresponding to γ-Al_2O_3 can be observed, which indicates the formation of poorly crystalline. Typical features of molybdenum and nickel oxides are absent, which

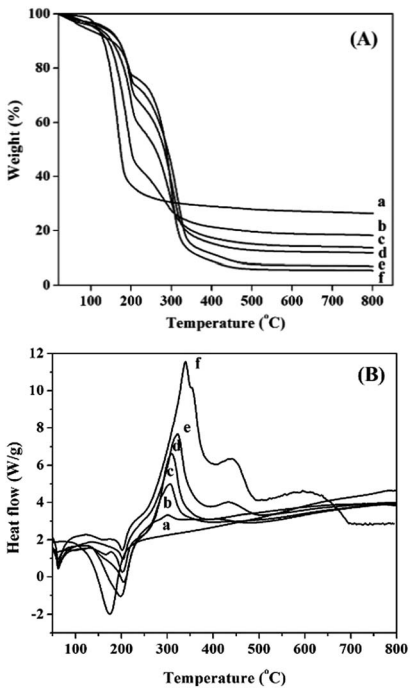

Fig. 1 TG curves (A) and DSC curves (B) of the NiMoAl-*x* precursors measured by TGA/DSC: (a) NiMoAl-0, (b) NiMoAl-2, (c) NiMoAl-6, (d) NiMoAl-10, (e) NiMoAl-15, and (f) NiMoAl-20.

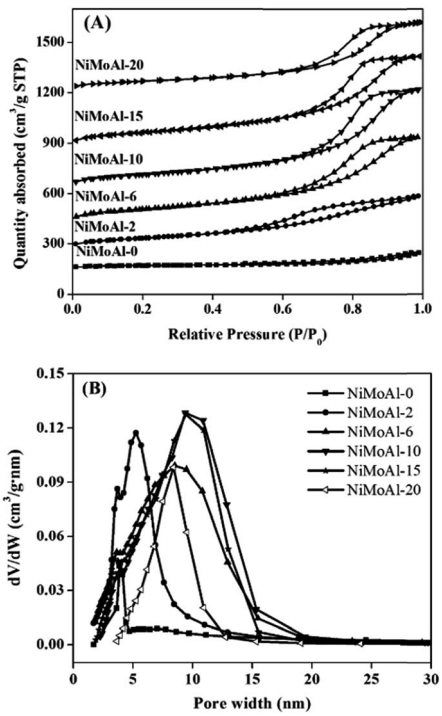

Fig. 2 Nitrogen adsorption–desorption isotherms (A) and pore size distributions (B) of the NiMoAl-*x* catalysts.

This journal is © The Royal Society of Chemistry 2017

Open Access Article. Published on 27 November 2017. Downloaded on 2/15/2026 4:36:53 AM. This article is licensed under a Creative Commons Attribution 3.0 Unported Licence.

Table 1 Summary of the several typical properties of the NiMoAl-*x* catalysts

	NiMoAl-0	NiMoAl-2	NiMoAl-6	NiMoAl-10	NiMoAl-15	NiMoAl-20	$NiMo/Al_2O_3$ (imp)
S_{BET} ($m^2\ g^{-1}$)[a]	72	306	384	407	420	243	250
V_p ($cm^3\ g^{-1}$)[b]	0.15	0.52	0.84	0.96	0.88	0.66	0.57
D_m (nm)[c]	4.0	5.3	8.6	10.0	9.9	8.4	8.1
Mo/Al ($\times 10^2$)[d]	3.4	3.9	3.7	3.9	4.1	4.0	4.5
Ni/Al ($\times 10^2$)[d]	4.3	2.6	4.4	5.0	5.4	2.5	3.4
S/Al ($\times 10^2$)[d]	8.6	8.4	11.0	12.3	13.2	9.1	12.3
Ni/(Ni + Mo)[d]	0.56	0.40	0.54	0.56	0.57	0.38	0.43
$Mo_{sul.}$ (%)[d]	60.7	75.9	86.9	89.0	89.8	89.5	81.2
L (nm)[e]	4.2	3.6	3.5	3.0	2.9	3.7	4.4
N[e]	2.8	2.5	2.4	2.2	2.1	1.9	3.4

[a] BET surface area. [b] Pore volume. [c] Most probable pore diameter. [d] Atomic ratio, obtained by XPS. [e] Determined by statistical analysis of HRTEM images.

can be due to the high dispersion of nickel and molybdenum species. For the sulfide catalysts, the weak and broad XRD peaks at 14.4°, 33.5°, and 58.6° (JCPDS card 37-1492) can be identified, which corresponding to (002), (101) and (110) crystal planes of MoS_2, respectively. The broad diffraction peaks indicate that no aggregated particles were formed after sulfurization and that there was a high dispersion of active components over the Al_2O_3 support surface.

3.3. Reducibility and surface composition

H_2-TPR characterization of the as-prepared oxide NiMoAl-*x* catalysts is shown in Fig. 3. For all the catalysts, three main H_2-consumption peaks could be clearly identified. On the basis of the previous reports, the first peak between 400 °C and 500 °C, which slightly shifted to lower temperature with increasing PEG addition, could be associated to the reduction ($Mo^{6+} \rightarrow Mo^{4+}$) of highly dispersed octahedral Mo species.[23] The second signal, identified in the temperature range of 500–700 °C, could be ascribed to oxidic Ni^{2+} species in weak interaction with the alumina. The high-temperature H_2-consuming peak between 750 °C and 900 °C is related to the second step of reduction of octahedral Mo species and the first step reduction of tetrahedral coordinated monomeric Mo species, which strongly bonded to the alumina support or enwrapped by alumina. It can be seen that a fraction of Mo oxide species possibly incorporated into alumina bulk phase, which are difficult to be reduced.

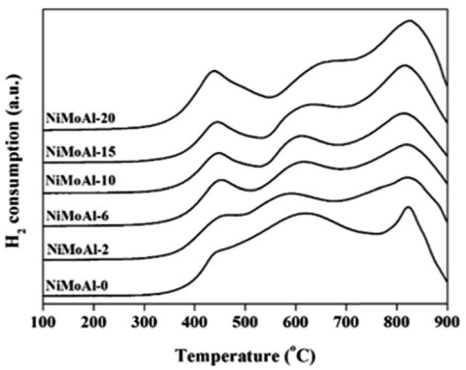

Fig. 3 H_2-TPR patterns of the oxide NiMoAl-*x* catalysts.

XPS spectra of the sulfided NiMoAl-*x* catalysts with different PEG addition were collected and decomposed. Mo 3d spectra of the catalysts are shown in S-Fig. 4,† and the related parameters are listed in Table 2. For Mo 3d spectra, 3 different contributions corresponding to MoS_2, MoO_xS_y, and Mo oxide species were determined according to binding energy values reported in previous works.[24] The three Mo 3d doublets are as follows: (1) the binding energy at approximately 228.7 eV (Mo^{4+} $3d_{5/2}$) associated with MoS_2 species, (2) the binding energy at 230.6 ± 0.2 eV (Mo^{5+} $3d_{5/2}$) correlated with a Mo oxy-sulfide species, and (3) the binding energy at 232.6 ± 0.2 eV (Mo^{6+} $3d_{5/2}$) related to Mo oxide species strongly bonded to alumina or enwrapped by alumina that were not completely sulfided. Furthermore, a broad peak at approximately 226.0 eV was assigned to the S 2s line and subtracted from the total spectrum of Mo 3d. For the NiMoAl-0 catalyst, a high percentage of MoO_x (Mo^{6+}) was measured, and the MoS_2 species represented only about 60.7%. However, the atomic percentage of Mo^{4+} in the sulfide phase increases significantly (from 60.7% to 89.5%) with the increase in the PEG content, demonstrating that the addition of PEG considerably improves the sulfidation and reducibility of Mo species.

Ni 2p XPS spectra of the sulfided NiMoAl-*x* catalysts are shown in S-Fig. 5.† Ni $2p_{3/2}$ envelope was decomposed by considering three major contributions. The binding energy at 853.5–854 eV corresponds to NiMoS phase. The peak at approximately 856.1 eV corresponds to Ni oxide species, including $NiAl_2O_4$ and NiO_x that

Table 2 XPS parameters of the different contributions of Mo 3d obtained for the sulfide NiMoAl-*x* catalysts

	Mo^{4+}		Mo^{5+}		Mo^{6+}	
Catalyst	BE (eV)	% atom	BE (eV)	% atom	BE (eV)	% atom
NiMoAl-0	228.8	60.7	230.7	16.2	232.7	23.1
NiMoAl-2	228.5	75.9	230.5	8.0	232.5	16.1
NiMoAl-6	229.0	86.9	230.6	4.6	232.8	8.5
NiMoAl-10	228.8	89.0	230.6	2.5	232.6	8.5

Open Access Article. Published on 27 November 2017. Downloaded on 2/15/2026 4:36:53 AM. This article is licensed under a Creative Commons Attribution 3.0 Unported Licence.

were strongly bonded to alumina support or enwrapped by alumina. Ni may also exist as NiS_x (Ni_3S_2, Ni_9S_8, and NiS), which is located at 853.0 ± 0.1 eV.[25] The relative quantities of Ni species (NiMoS, NiS_x, and Ni oxide) are reported in Table 3. The proportion of NiMoS phase, which is assumed to be the active phase for catalytic HDS, increases with PEG addition. A higher proportion of the NiMoS phase is obtained for the NiMoAl-15 sample, in which 76.3% of Ni atoms are engaged as compared to 65.1% in NiMoAl-0. The proportion of Ni oxide phase decreases with the increase of PEG amount, which can be attributed to the reduction of difficult-to-reduce species due to the blocking of PEG. These results suggested the presence of PEG suppresses the incorporation of Mo species into alumina bulk phase.

The integrated areas for Al 2p, Mo 3d, Ni 2p and S 2p peaks of the sulfided catalysts were used to calculate the atomic concentration ratios of Mo, Ni and S over Al. As shown in Table 1, the surface atomic ratio of Mo/Al increases with increasing PEG addition, which should be attributed to the transfer of Mo atoms from the bulk phase to the surface phase. However, Ni/(Ni + Mo) and Ni/Al ratios both reached a maximum value at a PEG/alumina weight ratio of about 15, in line with surface atomic ratio of S/Al. The Mo sulfidation degree ($Mo_{sul.}$) of NiMoAl-*x* catalysts was correlated with the fraction of Mo^{4+} determined by the decomposition of Mo 3d XPS spectra. The Mo sulfidation degree increases significantly with PEG addition, indicating that the addition of PEG considerably improve the sulfidability of Mo.

3.4. Morphology and dispersion of MoS_2 clusters

The external morphologies of the NiMoAl-*x* and $NiMo/Al_2O_3$ are presented in S-Fig. 6.† NiMoAl-0 with large particle size is mainly formed by the accumulation of flakes, and has a smooth surface, whereas NiMoAl-*x* (x = 6, 10, 15, 20) catalysts seem to be formed by the agglomeration of the uniform spherical particles with the size of 10 nm.

TEM characterization of the sulfided NiMoAl-*x* and $NiMo/Al_2O_3$ catalysts was performed for the determination of the MoS_2 dispersion and crystallites. Representative HRTEM micrographs of the catalysts are shown in S-Fig. 7.† Typical MoS_2 fringes with 6.2 Å interplanar distance are observed in all the micrographs of the sulfided catalysts. The slab lengths and stacking layer numbers of MoS_2 slabs on the sulfided NiMoAl-*x* catalysts were obtained through statistical analyses based on at least 20 images of 500–600 slabs taken from the different parts of each catalyst. The average layer number (N) and the average slab length (L) have been calculated according to the first moment of the distribution:[26]

$$L = \sum_{i=1}^{x} x_i l_i \Big/ \sum_{i=1}^{x} x_i \quad (1)$$

$$N = \sum_{i=1}^{y} y_i N_i \Big/ \sum_{i=1}^{y} y_i \quad (2)$$

where l_i is the length of slab i, N_i is the layer number of slab i, x_i is the number of slabs with length l_i, and y_i is the number of slabs with N_i layers.

The statistical results of the length and stacking layer number distributions of the MoS_2 slabs over the sulfided NiMoAl-*x* catalysts are showed in Fig. 4. Over 45% of the observed MoS_2 crystals are longer than 4 nm on the NiMoAl-0 catalyst, while the percentage decreases with increasing PEG content, as a result, the average slab length of MoS_2 gradually reduces. However, when the amount of PEG increases to 20 (NiMoAl-20), more MoS_2 crystals longer than 4 nm are detected. The NiMoAl-15 catalyst shows an average MoS_2 slabs length of 2.9 nm, which is much shorter than that of $NiMo/Al_2O_3$ catalyst prepared by impregnation method (L, Table 1). Particularly, the NiMoAl-15 catalyst exhibits the most centralized length distribution, more than 70% of the observed MoS_2 crystals length is between 2 nm and 4 nm. The stacking layer number distributions show that the proportion of multilayered structures (>4) increases with increasing PEG addition, which results an increase in the average stacking layer number (N, Table 1).

Table 3 XPS parameters of the different contributions of Ni 2p obtained for the sulfide NiMoAl-*x* catalysts

	NiMoS		NiS_x		NiO_x	
Catalyst	BE (eV)	% atom	BE (eV)	% atom	BE (eV)	% atom
NiMoAl-0	853.6	65.1	853.1	2.7	855.9	32.1
NiMoAl-2	853.5	68.0	853.0	3.4	855.9	28.6
NiMoAl-6	853.7	71.8	853.0	1.8	856.2	26.4
NiMoAl-10	853.9	75.2	853.2	0.8	856.3	23.8
NiMoAl-15	853.9	76.3	853.0	1.8	856.0	21.9
NiMoAl-20	854.0	75.2	853.1	1.2	856.3	23.6

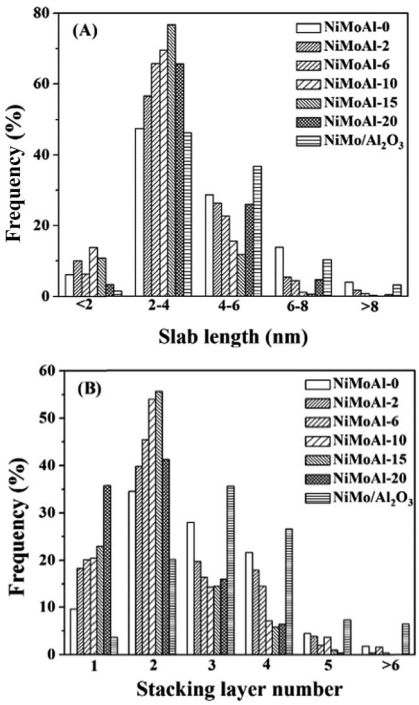

Fig. 4 Slab lengths (A) and stacking layer number (B) distributions of MoS_2 crystallites on the sulfide NiMoAl-*x* and $NiMo/Al_2O_3$ catalysts.

 This journal is © The Royal Society of Chemistry 2017

Open Access Article. Published on 27 November 2017. Downloaded on 2/15/2026 4:36:53 AM. This article is licensed under a Creative Commons Attribution 3.0 Unported Licence.

Additionally, the stacking layer number distribution of the NiMoAl-15 catalyst is the most homogenous, with over 70% of MoS_2 slabs having 2 to 3 layers. Compared with NiMo/Al_2O_3, all NiMoAl-*x* catalysts show lower average stacking layer (1.9–2.8), which suggests a better MoS_2 dispersion. The addition of PEG can block the aggregation of metals and support, and improve Mo dispersion.[27,28] Thus, more active MoS_2 can be generated.

The average fraction of Mo atoms on the edge surface of the MoS_2 crystals, denoted as f_{Mo}, is a dispersion indicator of the active surface of the crystal. The f_{Mo} value is determined from eqn (3), by assuming that the MoS_2 crystals are perfect hexagons.[29] In eqn (3), the numerator is the number of atoms in the active surface (edges) and the denominator is the total number of Mo atoms in the crystal; t is the total number of slabs shown in the HRTEM images, and n_i is the number of Mo atoms in one edge, determined from the slab length L as shown in eqn (4)

$$f_{MO} = \sum_{i=1}^{t}(6n_i - 6) \Big/ \sum_{i=1}^{t}(3n_i^2 - 3n_i + 1) \quad (3)$$

$$n_i = L/6.4 + 0.5 \quad (4)$$

The f_{Mo} values in Table 1 show a noticeably higher MoS_2 dispersion on the sulfided NiMoAl-*x* catalysts prepared using PEG, as compared to the NiMo/Al_2O_3 catalyst. The MoS_2 dispersion over the NiMoAl-*x* catalysts increases from 0.23 to 0.34 with increasing PEG content.

3.5. HDS performance of the NiMoAl-*x* catalysts

The HDS reaction results of dibenzothiophene (DBT) for the NiMoAl-*x* catalysts are reported in Table 4. The conversion of DBT occurs through two parallel routes: the direct desulfurization pathway (DDS) yields mainly biphenyl (BP), whereas the hydrogenation route (HYD) generates cyclohexylbenzene (CHB) and dicyclohexyl (DCH). The specific rate of DBT HDS increased with increasing PEG addition and peaked at NiMoAl-15, decreasing thereafter. Compared to NiMo/Al_2O_3 catalyst, the DBT HDS conversion was 10 percent higher for NiMoAl-15 catalyst under the same conditions. It is noted that the CHB selectivity over the NiMoAl-15 catalyst is higher than that over NiMoAl-0 and NiMoAl-20 catalysts. As a result, the NiMoAl-15 catalyst shows a large HYD/DDS ratio, and the total HDS activities of DBT over the NiMoAl-*x* catalysts have the same changing tendency as HYD/DDS ratio, which can be attributed to more accessible NiMoS edge sites. However, the selectivity of BP produced *via* the DDS pathway is much higher than that of CHB and DCH formed through the HYD route, which was similar to the findings of previous studies.[30] This feature should be due to the low hydrogen pressure and high liquid hourly space velocity (LHSV).

Table 4 Initial activities and product distributions for dibenzothiophene HDS over the NiMoAl-*x* and NiMo/Al_2O_3 catalysts[a]

Catalyst	R^b (10^{-6} mol g^{-1} s^{-1})	Product selectivity[c] (%)			
		BP	CHB	DCH	HYD/DDS
NiMoAl-0	0.47	92.3	5.4	2.3	0.083
NiMoAl-10	1.33	90.5	7.8	1.7	0.105
NiMoAl-15	1.41	89.8	8.5	1.7	0.114
NiMoAl-20	1.09	91.9	6.1	2.0	0.088
NiMo/Al_2O_3	1.25	90.9	7.3	1.8	0.100

[a] Reaction conditions: temperature, 300 °C; H_2 pressure, 2.0 MPa; LHSV, 12 h^{-1}; H_2/liquid (v/v), 600; feed, 2 wt% DBT in decalin. [b] Initial specific rate (moles of DBT transformed per second and per gram of catalyst). [c] DDS, direct desulfurization pathway; HYD, hydrogenation pathway; BP, biphenyl; CHB, cyclohexylbenzene; DCH, dicyclohexyl.

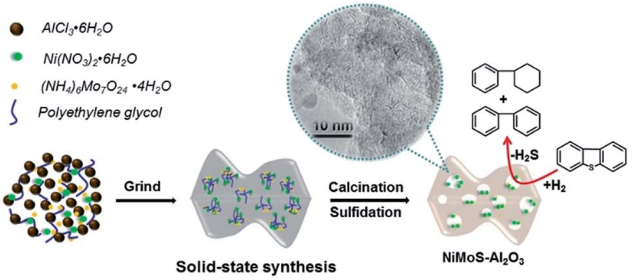

Fig. 5 Schematic illustration of the solid-state synthesis of mesoporous NiMoS–Al_2O_3 catalysts for dibenzothiophene hydrodesulfurization.

3.6. Effect of PEG on catalyst structure and HDS activity

As shown in Fig. 5, the solid-state method using PEG as additive permit to synthesize highly active Al_2O_3 supported NiMo HDS catalysts. The addition of PEG results in large surface area and pore volume, which allow the catalyst to expose more active sites. Indeed, the addition of PEG improves the reducibility and sulfidability of Mo, as proved by TPR and XPS results, which suggests a weak metal–support interaction. However, a larger Mo dispersion can be observed from the HRTEM images with PEG addition, which can be attributed to suppression of active metal aggregation by PEG blocking.[27,28] As previous studies described, this positive effect may be caused by the fact that there is a coordination/interaction between numerous hydroxyl (OH) in PEG and active metals on the alumina support. During the drying step, higher dispersion of Ni and Mo precursors was maintained on the alumina surface even after water removal, since PEG has higher boiling point than water. These results are the major factors for the significant improvement in the HDS activity of dibenzothiophene.

4. Conclusions

In the present work, we develop a simple and solvent-free solid-state route for synthesizing Al_2O_3 supported NiMo catalysts with different PEG addition, which also can be used to synthesis Al_2O_3 supported other metal catalysts. An appropriate amount of addition of polyethylene glycol (PEG) can dramatically increases specific surface area and pore volume of the catalyst, and improves Mo sulfidability and active MoS_2 dispersion by

Open Access Article. Published on 27 November 2017. Downloaded on 2/15/2026 4:36:53 AM. This article is licensed under a Creative Commons Attribution 3.0 Unported Licence.

blocking the aggregation among metals. As a result, dibenzothiophene HDS activity enhanced with increasing PEG addition and peaked at NiMoAl-15, decreasing thereafter. Compared with the $NiMo/Al_2O_3$ catalyst prepared by incipient wetness co-impregnation, NiMoAl-15 exhibited a significantly higher HDS activity. Concerning the selectivity, the HYD/DDS ratio is parallel to the activities of the NiMoAl-*x* catalysts for the HDS of DBT, which is in good agreement with the total population of Ni–Mo–S active sites.

Conflicts of interest

There are no conflicts to declare.

Acknowledgements

This work is supported by the National Natural Science Foundation of China (21373168, 21473143, 21773194 and 21703179) and the Science and Technology Foundation of Guangxi (14125008-2-10).

Notes and references

1 C. Song, *Catal. Today*, 2003, **86**, 211–263.
2 R. Huirache-Acuna, B. Pawelec, E. M. Rivera-Munoz, R. Guil-Lopez and J. L. G. Fierro, *Fuel*, 2017, **198**, 145–158.
3 R. K. Kaila, A. Gutiérrez and A. O. I. Krause, *Appl. Catal., B*, 2008, **84**, 324–331.
4 Y. Saih, M. Nagata, T. Funamoto, Y. Masuyama and K. Segawa, *Appl. Catal., A*, 2005, **295**, 11–22.
5 J. C. Morales-Ortuno and T. E. Klimova, *Fuel*, 2017, **198**, 99–109.
6 Z. Vít, D. Gulková, L. Kaluža, S. Bakardieva and M. Boaro, *Appl. Catal., B*, 2010, **100**, 463–471.
7 J. A. Schaidle, N. M. Schweitzer, O. T. Ajenifujah and L. T. Thompson, *J. Catal.*, 2012, **289**, 210–217.
8 Q. Guan and W. Li, *Catal. Sci. Technol.*, 2012, **2**, 2356–2360.
9 M. Rana, J. Ramirez, A. Gutierrezalejandre, J. Ancheyta, L. Cedeno and S. Maity, *J. Catal.*, 2007, **246**, 100–108.
10 T. E. Klimova, D. Valencia, J. A. Mendoza-Nieto and P. Hernández-Hipólito, *J. Catal.*, 2013, **304**, 29–46.
11 J. A. Toledo-Antonio, M. A. Cortes-Jacome, J. Escobar-Aguilar, C. Angeles-Chavez, J. Navarrete-Bolanos and E. Lopez-Salinas, *Appl. Catal., B*, 2017, **213**, 106–117.
12 J. Escobar, M. C. Barrera, J. A. Toledo, M. A. Cortés-Jácome, C. Angeles-Chávez, S. Núñez, V. Santes, E. Gomez, L. Diaz and E. Romero, *Appl. Catal., B*, 2009, **88**, 564–575.
13 S. Liu, X. Liang, J. Zhang and B. Chen, *Catal. Sci. Technol.*, 2017, **7**, 466–480.
14 Y. Fan, H. Xiao, G. Shi, H. Y. Liu, Y. Qian, T. H. Wang, G. B. Gong and X. J. Bao, *J. Catal.*, 2011, **279**, 27–35.
15 J. Quartararo, J. P. Amoureux and J. Grimblot, *J. Mol. Catal. A: Chem.*, 2000, **162**, 353–365.
16 M. Zhang, T. Yang, R. Zhao and C. Liu, *Appl. Catal., A*, 2013, **468**, 327–333.
17 L. M. Ren, Q. M. Wu, C. G. Yang, L. F. Zhu, C. J. Li, P. L. Zhang, H. Y. Zhang, X. J. Meng and F. S. Xiao, *J. Am. Chem. Soc.*, 2012, **134**, 15173–15176.
18 X. Guo, D. Mao, G. Lu, S. Wang and G. Wu, *Catal. Commun.*, 2011, **12**, 1095–1098.
19 W. K. Lai, W. J. Song, L. Q. Pang, Z. F. Wu, J. J. Li, X. D. Yi and W. P. Fang, *J. Catal.*, 2013, **303**, 80–91.
20 W. K. Lai, L. Q. Pang, J. B. Zheng, J. J. Li, Z. F. Wu, X. D. Yi and W. P. Fang, *Fuel Process. Technol.*, 2013, **110**, 8–16.
21 H. Knozinger and P. Ratnasamy, *Catal. Rev.: Sci. Eng.*, 1978, **17**, 31–69.
22 M. A. A. Elmasry, A. Gaber and E. M. H. Khater, *J. Therm. Anal.*, 1998, **52**, 489–495.
23 L. Qu, W. Zhang, P. J. Kooyman and R. Prins, *J. Catal.*, 2003, **215**, 7–13.
24 B. Guichard, M. Roy-Auberger, E. Devers, C. Legens and P. Raybaud, *Catal. Today*, 2008, **130**, 97–108.
25 T. K. T. Ninh, L. Massin, D. Laurenti and M. Vrinat, *Appl. Catal., A*, 2011, **407**, 29–39.
26 D. Zuo, M. Vrinat, H. Nie, F. Maugé, Y. Shi, M. Lacroix, Y. H. Shi, M. Lacroix and D. D. Li, *Catal. Today*, 2004, **93–95**, 751–760.
27 R. Iwamoto, N. Kagami and A. Iino, *J. Jpn. Pet. Inst.*, 2005, **48**, 237–242.
28 R. Iwamoto, N. Kagami, Y. Sakoda and A. Iino, *J. Jpn. Pet. Inst.*, 2005, **48**, 351–357.
29 E. J. M. Hensen, P. J. Kooyman, Y. Meer, A. M. Kraan, V. H. J. Beer, J. A. R. Veen and R. A. Santen, *J. Catal.*, 2001, **199**, 224–235.
30 P. Schacht, S. Ramírez and J. Ancheyta, *Energy Fuels*, 2009, **23**, 4860–4865.

 This journal is © The Royal Society of Chemistry 2017